Aalborg Universitet

AALBORG UNIVERSITY

Programmed seasonal brain shrinkage in the common shrew via water loss without cell death

Baldoni, Cecilia; Reisert, Marco; Smith, Bethany; Lázaro, Javier; Zeng, Yuanyuan; Thomas, William R; Hertel, Moritz; Dávalos, Liliana M; Nieland, John; Dechmann, Dina K N; von Elverfeldt, Dominik

Published in:
Current biology : CB

DOI (link to publication from Publisher):
10.1016/j.cub.2025.08.015

Creative Commons License
CC BY 4.0

Publication date:
2025

Document Version
Publisher's PDF, also known as Version of record

Link to publication from Aalborg University

Citation for published version (APA):
Baldoni, C., Reisert, M., Smith, B., Lázaro, J., Zeng, Y., Thomas, W. R., Hertel, M., Dávalos, L. M., Nieland, J., Dechmann, D. K. N., & von Elverfeldt, D. (2025). Programmed seasonal brain shrinkage in the common shrew via water loss without cell death. *Current biology : CB*, *35*(19), 4642-4650.e3. https://doi.org/10.1016/j.cub.2025.08.015

General rights
Copyright and moral rights for the publications made accessible in the public portal are retained by the authors and/or other copyright owners and it is a condition of accessing publications that users recognise and abide by the legal requirements associated with these rights.

- Users may download and print one copy of any publication from the public portal for the purpose of private study or research.
- You may not further distribute the material or use it for any profit-making activity or commercial gain
- You may freely distribute the URL identifying the publication in the public portal -

Take down policy
If you believe that this document breaches copyright please contact us at vbn@aub.aau.dk providing details, and we will remove access to the work immediately and investigate your claim.

Downloaded from vbn.aau.dk on: December 10, 2025

Article

Current Biology

Programmed seasonal brain shrinkage in the common shrew via water loss without cell death

Graphical abstract

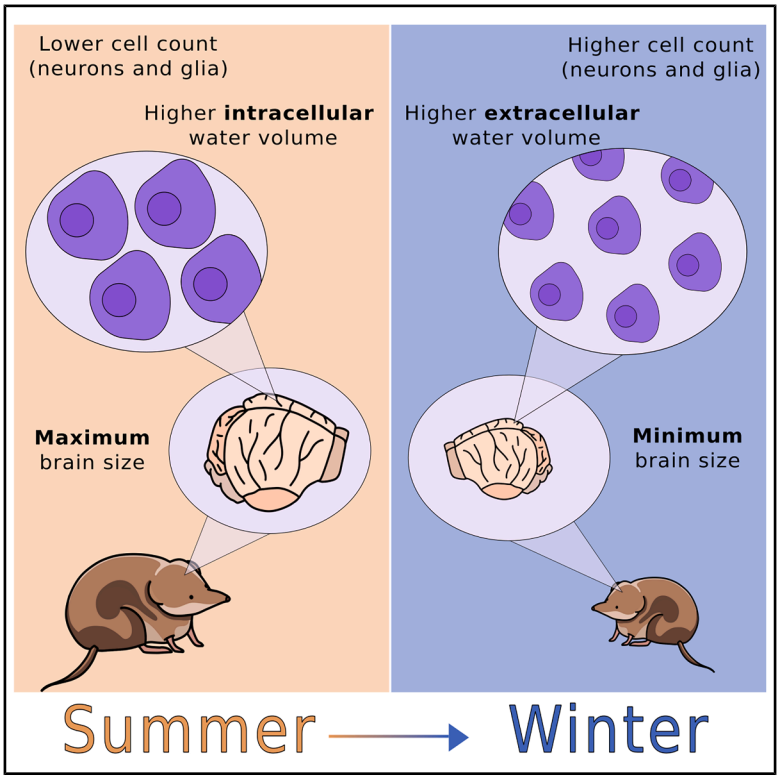

Highlights

- Seasonal brain shrinkage in shrews occurs via cell shrinkage, not cell death
- Brain intracellular water decreases and extracellular water increases in winter
- Neuronal and glial numbers remain stable across seasons, preserving brain function
- Aquaporin-4 expression declines in cortex and hippocampus in winter

Authors

Cecilia Baldoni, Marco Reisert, Bethany Smith, ..., John Nieland, Dina K.N. Dechmann, Dominik von Elverfeldt

Correspondence

cbaldoni@ab.mpg.de

In brief

Baldoni et al. reveal that common shrews naturally shrink their brains in winter by reducing cell size and water content rather than through cell loss, maintaining brain function through reversible, energy-saving adaptations.

Baldoni et al., 2025, Current Biology *35*, 4642–4650
October 6, 2025 © 2025 The Author(s). Published by Elsevier Inc.
https://doi.org/10.1016/j.cub.2025.08.015

CellPress

CellPress
OPEN ACCESS

Current Biology

Article

Programmed seasonal brain shrinkage in the common shrew via water loss without cell death

Cecilia Baldoni,[1,2,11,*] Marco Reisert,[3,4] Bethany Smith,[5] Javier Lázaro,[6] Yuanyuan Zeng,[7] William R. Thomas,[8] Moritz Hertel,[9] Liliana M. Dávalos,[8,10] John Nieland,[7] Dina K.N. Dechmann,[1,2] and Dominik von Elverfeldt[3,4]

[1]Max Planck Institute of Animal Behavior, Department of Migration, Radolfzell am Bodensee 78315, Germany
[2]Department of Biology, University of Konstanz, Konstanz 78464, Germany
[3]Division of Medical Physics, Department of Diagnostic and Interventional Radiology, University Medical Center Freiburg, Faculty of Medicine, University of Freiburg, Freiburg 79106, Germany
[4]Department of Stereotactic and Functional Neurosurgery, Medical Center of Freiburg University, Medical Faculty of Freiburg University, Freiburg 79106, Germany
[5]School of Biodiversity, One Health and Veterinary Medicine, University of Glasgow, Glasgow G61 1QH, UK
[6]Javier Lázaro Scientific and Wildlife Illustration, Noasca 10080, Italy
[7]Department of Health Science and Technology, Aalborg University, Aalborg 9220, Denmark
[8]Department of Ecology & Evolution, Stony Brook University, Stony Brook, NY 11794, USA
[9]Max Planck Institute for Biological Intelligence, Department for Neurobehaviour, Seewiesen 82319, Germany
[10]Consortium for Inter-Disciplinary Environmental Research, Stony Brook University, Stony Brook, NY 11794, USA
[11]Lead contact
*Correspondence: cbaldoni@ab.mpg.de
https://doi.org/10.1016/j.cub.2025.08.015

SUMMARY

Brain plasticity, the brain's inherent ability to adapt its structure and function, is crucial for responding to environmental challenges but is usually not linked to a significant change in size. A striking exception to this is Dehnel's phenomenon, where seasonal reversible brain-size reduction occurs in some small mammals to decrease metabolic demands during resource-scarce winter months. Despite these volumetric changes being well documented, the specific microstructural alterations that facilitate this adaptation remain poorly understood. Our study employed diffusion microstructure imaging (DMI) to explore these changes in common shrews, revealing significant alterations in water diffusion properties such as increased mean diffusivity and decreased fractional anisotropy, leading to decreased water content inside brain cells during winter. These findings confirm that brain-size reduction correlates with a decrease in cell size, as our data indicate no reduction in cell numbers, showcasing a reorganization of brain tissue that supports survival without compromising brain function. These findings extend our understanding of neuronal resilience and may inform future research on regenerative mechanisms, particularly during the spring regrowth phase, offering potential strategies relevant to neurodegenerative disease.

INTRODUCTION

Brain plasticity is the remarkable ability to reorganize the structure, functions, and connections of the brain in response to environmental demands, learning, or recovery from injury. This adaptive capacity is essential for survival in fluctuating environments, enabling the brain to maintain optimal function despite changes in external conditions.[1,2] These changes encompass structural and functional reorganization and metabolic shifts that help the brain cope with various stressors.[3] For example, recent evidence suggests that brain structure and properties can change seasonally, potentially influencing neurological disorders and cognitive processes.[4,5]

One extraordinary instance of brain plasticity in response to changing environments is Dehnel's phenomenon, first described by Dehnel[6] and later confirmed in the common shrew (*Sorex araneus*) by Bielak and Pucek.[7] This phenomenon involves a considerable decrease in body and brain volume from summer to winter, followed by spring regrowth. This seasonal plasticity has been observed in small mammal species with high metabolisms and year-round activity in cold climates, and it is likely an adaptation to winter as the shrinkage starts in autumn before the onset of winter.[8] By reducing overall size, and especially the size of expensive organs such as the brain, the amount of food required for survival is reduced in winter, when food sources are scarce, more sparsely spread, and slower to replenish.[9,10] With low fat stores and a high metabolic rate, these animals must efficiently locate sufficient amounts of food without wasting energy searching in depleted areas.[11] To date, Dehnel's phenomenon has been observed in European moles,[12] stoats and weasels,[13] and the subfamily of red-toothed shrews.[14] There are also seasonal changes in brain mass reported in some rodents, such as red-backed voles and striped mice,[15,16] but these have not yet been confirmed as true cases of Dehnel's phenomenon. Among the red-toothed shrews, the common shrew (*Sorex araneus*) is considered the model species for this unique form of

 © 2025 The Author(s). Published by Elsevier Inc.
This is an open access article under the CC BY license (http://creativecommons.org/licenses/by/4.0/).

brain plasticity.[6,8] In a population in Southern Germany, common shrews reach their minimum mass at the end of February, with brains 10%–26% smaller compared with their summer size.[17] The brain begins to grow again in spring and a second, smaller maximum is reached in summer,[17] as individuals reach sexual maturity (June), shortly before reproduction, after which shrews rapidly senesce and die. This reversible change in brain size represents a natural response to environmental pressures and a potentially critical adaptation for energy conservation and survival during harsh winters.

Extensive research has quantified the volumetric changes associated with Dehnel's phenomenon, noting a significant reduction in the brain weight and water content in the common shrew during winter compared with summer.[18] This reduction is accompanied by increased dry matter content, indicating that dehydration plays a significant role in these seasonal brain weight variations.[18] Additionally, seasonal lipid contents change, with the lowest levels in juveniles during summer, an increase during winter and spring, and a subsequent decrease in adults during summer and autumn. Altered water and lipid content suggest that the brain undergoes significant structural changes to maintain function during harsh conditions, which likely contributes to the observed reduction in neuronal structures by Lázaro et al.[19] They found a general decrease in soma size and total dendrite volume in the caudoputamen and anterior cingulate cortex, but this at most partially explains the overall tissue shrinkage observed in winter.

Despite these findings, significant gaps remain in understanding the microstructural changes underlying these volumetric adaptations. Specifically, the precise quantification of water molecules and the fundamental mechanisms by which they move within the brain during this seasonal transition have yet to be fully explored. Thus, the physiological basis of Dehnel's phenomenon remains unknown. One potential mediator of this process is aquaporin-4 (AQP4), a water channel widely distributed in the mammalian brain within the glymphatic system.[20] The glymphatic system facilitates the clearance of metabolic waste through interstitial fluid flow (ISF), regulated by AQP4.[21,22] Disruptions in AQP4 expression impair this clearance, leading to the deposition of β-amyloid, which aligns with the pathological mechanisms observed in Alzheimer's disease and other neurodegenerative diseases.[22,23] Conversely, increased AQP4 activity has been shown to enhance ISF and cerebrospinal fluid (CSF) turnover.[24]

AQP4's role in regulating water movement highlights its potential involvement in seasonal changes in water content during Dehnel's phenomenon. Measuring how water redistributes within the brain can provide insights into these adaptations. Brain diffusion properties, which describe the behavior of water molecules moving within brain tissue, offer a non-invasive way to quantify tissue structure and dynamics. This movement can be measured with advanced imaging techniques like diffusion-weighted MRI (DW-MRI), which allows for the non-invasive quantification of tissue architecture and structure through the use of endogenous water, making it a powerful tool in investigating local tissue microstructure.[25] Moreover, DW-MRI can distinguish between different tissue water compartments, such as intracellular water, extracellular water, and water in the microvascular system.[26] Key metrics derived from DW-MRI help quantify these diffusion characteristics. Fractional anisotropy (FA) is a measure of the directional uniformity of water diffusion. High FA values typically indicate healthy, well-organized neural tracts with highly directional water movement. Mean diffusivity (MD) quantifies the average rate of water diffusion within brain tissue. Lower MD values often point to denser tissue, whereas higher MD can signal less-restricted water movement, possibly due to tissue degradation. Axial diffusivity (aD) reflects water diffusion along the primary axis of neural fibers and is frequently employed to assess axonal integrity. A reduction in aD is generally linked to axonal injury. Radial diffusivity (rD) gauges diffusion perpendicular to the main axis of neural tracts and is sensitive to alterations in myelin structure. Increased rD values can suggest myelin breakdown.

In healthy brain tissue, diffusion is directional and restricted, indicative of intact microstructural integrity, better axonal coherence, density, and myelination.[27] Conversely, in neurodegenerative diseases, diffusion patterns become more random and less directional, resulting in lower FA and aD and higher MD.[28,29] These alterations in diffusion metrics are associated with loss of microstructural integrity and reduced tissue organization, reflecting breakdowns in neural pathways and myelin sheaths.[30,31] Additionally, AQP4 knockout mice exhibit a larger interstitial space on diffusion MRI compared with wild-type mice, which is likely due to the reduced ISF in the glymphatic system caused by the absence of AQP4.[32]

In the context of Dehnel's phenomenon, seasonal changes in brain tissue properties, reflected by variations in water content, might affect the overall cellular composition, potentially explaining the observed reduction in brain weight and increased dry matter content in winter, as documented by Pucek.[18] Although Dehnel's phenomenon represents an adaptive, reversible modification of brain structure as a response to environmental stress, it contrasts strongly with the irreversible changes observed in human neurodegenerative diseases, such as Alzheimer's disease, which are characterized by chronic, progressive, and irreversible loss of neural integrity. Interestingly, both conditions share a decline in cognitive performance as a common symptom,[33,34] suggesting that similar mechanisms related to disrupted water homeostasis might be involved. This similarity raises the question of whether the dysregulation of water diffusion could lead to cell dehydration and consequent cell death during Dehnel's phenomenon, mirroring the pathological processes observed in human neurodegeneration.

A previous study using antihistamine staining during peak stages of Dehnel's phenomenon found no indication of adult neurogenesis or cell death between stages of Dehnel's phenomenon.[35] In contrast, long-term field datasets confirm that Dehnel's phenomenon remains a consistent seasonal pattern in natural settings, despite some year-to-year variability,[36,37] suggesting that these cellular processes occur reliably under typical environmental fluctuations.

To address existing gaps in our understanding of seasonal brain adaptations, we employed diffusion microstructure imaging (DMI) on common shrews in their natural summer and winter phenotypes, representing their maximum and minimum brain sizes, respectively. DMI is an advanced DW-MRI technique that decomposes and identifies the diffusion characteristics of brain tissue into intra-axonal, extra-axonal, and free-water compartments.[38] Preliminary evidence has shown that

Table 1. Bayesian estimates of seasonal differences in regional brain volumes

Region	Estimate (Δ winter − summer)	Est. error	95% CI lower	95% CI upper
Amygdala	−0.303	0.029	−0.361	−0.246
Anterior olfactory nucleus	+0.002	0.008	-0.013	+0.017
Caudoputamen	−0.034	0.023	−0.079	+0.009
Cerebellum	**−2.31**	0.150	−2.60	−2.01
Hippocampus	**−2.00**	0.090	−2.18	−1.82
Midbrain	**+0.405**	0.088	+0.228	+0.578
Nucleus accumbens	−0.150	0.014	−0.178	−0.122
Neocortex	**−1.51**	0.136	−1.78	−1.25
Olfactory bulb	**−1.70**	0.091	−1.88	−1.52
Olfactory tubercle	−0.247	0.026	−0.298	−0.196
Piriform/Entorhinal cortices	−0.988	0.046	−1.08	−0.900
Pons/medulla	**−4.90**	0.164	−5.22	−4.57
Thalamus	−0.135	0.034	−0.201	−0.069

Estimated seasonal differences in regional brain volumes (winter − summer) based on Bayesian Gaussian models. Each brain region was modeled separately using volume as the response variable and season as a fixed effect, with a random intercept for individual ID. Negative values indicate smaller regional volume in winter compared with summer. Estimates are presented in mm^3 with 95% credible intervals.

multi-shell (multiple b values) high angular resolution diffusion imaging (HARDI) protocols can potentially yield more accurate diffusion metrics for DMI, particularly in distinguishing white and gray matter.[39,40] Although HARDI is commonly used in tractography applications, in our study it was employed to support the requirements of the DMI model, which necessitates multi-shell diffusion data for accurate estimation of microstructural properties across brain regions, including gray matter. To avoid missing short-lived periods of cell proliferation or death, which might occur outside fixed sampling points, we took a different approach than Bartkowska et al.[35] By quantifying total cell numbers in wild-caught shrews during both summer and winter, we aimed to capture the net seasonal differences in cell populations, regardless of when during the seasonal cycle those changes occurred.

We hypothesized two main mechanisms driving seasonal brain adaptations. First, we hypothesized that the observed volumetric changes in the shrew brain between seasons are driven by a reduction in cell size, consistent with the decrease in brain water content described by Pucek.[18] This shrinkage likely involves mechanisms regulating intracellular and extracellular water redistribution. Specifically, we hypothesized that the water channel protein AQP4 decreases in expression during winter. This reduction would align with energy-saving strategies and facilitate the redistribution of water by reducing water influx into cells, decreasing intracellular water volume, and increasing extracellular space. Second, following the results of Bartkowska and colleagues, we hypothesized that seasonal brain volume reductions occur without significant cell death, as evidenced by stable total cell numbers. This would suggest that volume reductions are achieved through non-degenerative processes, such as cell shrinkage and extracellular space expansion rather than permanent cellular loss.

These adaptations are expected to involve region-specific mechanisms of water management that help maintain structural and functional integrity under environmental challenges. By studying shrews, which exhibit these reversible adaptations, we aim to enhance our understanding of brain plasticity and resilience. This could provide valuable insights into mechanisms that counteract neurodegenerative processes, offering potential strategies to mitigate such diseases in humans.

RESULTS

Seasonal changes in brain and brain region volumes

We observed a significant reduction in total brain volume from summer to winter (estimate: −21.08 mm^3, 95% confidence interval [CI]: −21.51 to −20.67), confirming the presence of seasonal brain shrinkage in our MRI-based measurements. This corresponds to an ∼9% decrease, consistent with previous findings.[33] Region-specific models revealed significant volume reductions in most brain regions (Table 1). The most-affected areas included the pons and medulla (−4.90 mm^3, 95% CI: −5.22 to −4.57), cerebellum (−2.31 mm^3, 95% CI: −2.60 to −2.01), hippocampus (−2.00 mm^3), and neocortex (−1.51 mm^3). In contrast, the midbrain showed a slight increase (+0.41 mm^3) and the anterior olfactory nucleus remained stable (Table 1).

Seasonal effects on brain metrics

Estimates from the beta regression models are presented on the logit scale, which reflects the linear predictor of the beta-distributed outcome. Our results showed that seasonality significantly affected brain tissue microstructure (Figure 1; Table 2), with region-specific differences (supplemental information; Figures S1 and S2; Table S1, estimates reported in log-odds). Intracellular water volume fraction declined significantly from summer to winter, with a seasonal effect estimate of −0.184 (95% CI: −0.258, −0.110). At the same time, the extracellular water volume fraction increased significantly—but less than the intracellular water decreased—with the season change (0.310, 95% CI: 0.187, 0.432). rD, aD, and MD showed a comparable,

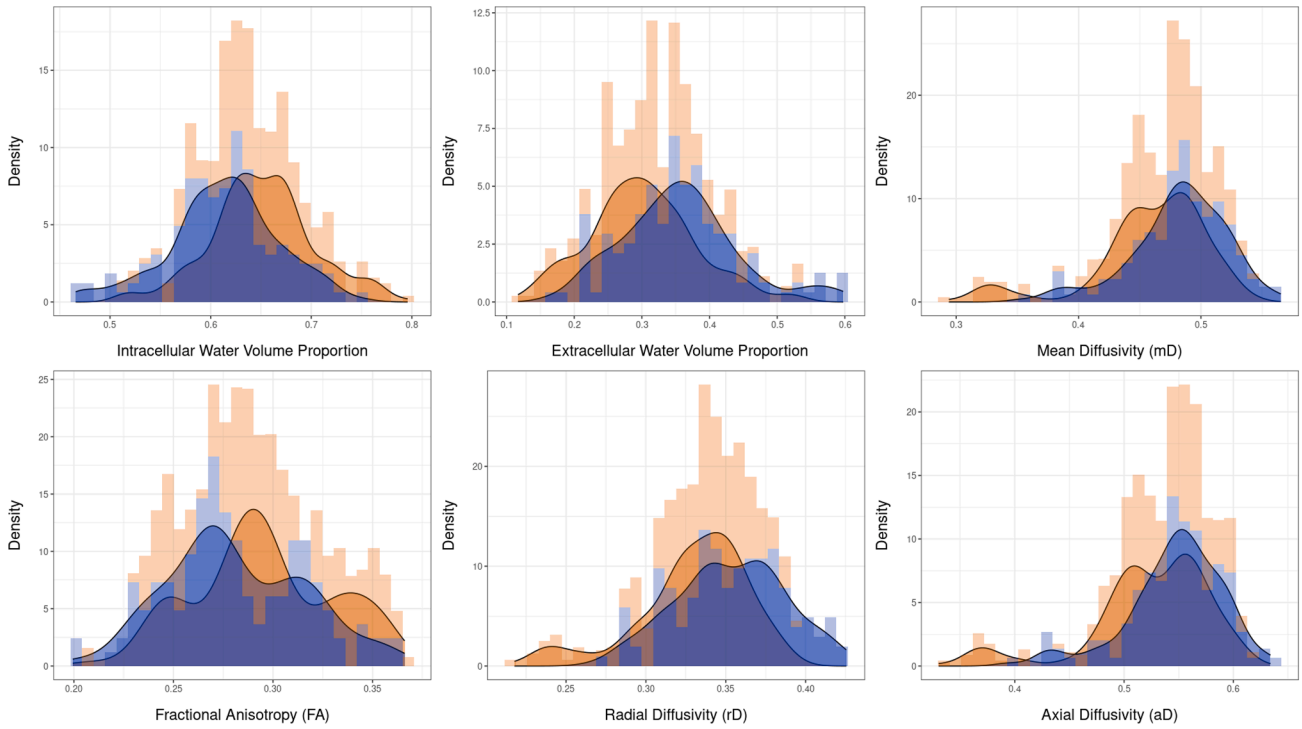

Figure 1. Seasonal differences in brain water diffusion metrics and volume proportions

Density distributions of water diffusion metrics and compartment volume proportions across summer (orange) and winter (blue), derived from Bayesian models. See also Figure S1 for distribution ranges by individual and Figure S2 for region-specific model results.

significant increase between summer and winter. CSF volume fraction decreased slightly, though not significantly (−0.103, 95% CI: −0.218, 0.007), and the seasonal effects between brain regions were generally not significant, with minor exceptions not showing consistent patterns across other metrics. Interestingly, the neocortex and cerebellum opposed the general trends in all metrics, although in the cerebellum the deviations were generally less pronounced than in the neocortex (see Table S1 for all brain regions by metric).

Table 2. Bayesian estimates of seasonal changes in brain diffusion metrics

Diffusion metric	Estimate	Est. error	Lower CI	Upper CI
Intracellular water volume fraction	−0.184	0.037	−0.258	−0.11
Extracellular water volume fraction	0.31	0.062	0.187	0.432
Mean diffusivity (MD)	0.097	0.033	0.032	0.164
Fractional anisotropy (FA)	−0.072	0.023	−0.119	−0.025
Axial diffusivity (aD)	0.092	0.035	0.022	0.161
Radial diffusivity (rD)	0.113	0.03	0.053	0.173
Cerebrospinal fluid (CSF) volume fraction	−0.103	0.057	−0.218	0.007

Estimated differences in brain tissue diffusion metrics between summer and winter. Negative values indicate a decrease from summer to winter; positive values indicate an increase.

Correlation of metrics between seasons

The results from the relative values (water fraction) of intracellular and extracellular water volume and CSF by brain region showed that increases in extracellular volume significantly reduced the intracellular water fraction in both seasons (estimate in log-odds: −2.93, 95% CI: −3.15 to −2.71 in summer; −2.69, 95% CI: −2.84 to −2.55 in winter; Table S2). Similarly, CSF volume also negatively affected intracellular volume (−0.58, 95% CI: −1.07 to −0.10 in summer; −0.65, 95% CI: −1.03 to −0.25 in winter). This implies that changes in the surrounding fluid volumes—extracellular and CSF—tended to significantly decrease the probability of intracellular space being occupied from summer to winter. The model assessing FA in relation to rD and aD showed that FA significantly declined with increasing rD in winter (−8.28, 95% CI: −8.90 to −7.67), while no such association was found in summer. Conversely, increases in aD were positively associated with FA in both seasons, with stronger effects in summer (5.04, 95% CI: 4.63–5.46) than winter (4.71, 95% CI: 4.26–5.13) (Table S3).

Correlation between metric changes and volume shrinkage

We examined whether changes in intracellular water, extracellular water, and CSF volume were associated with brain volume shrinkage across seasons. The model did not indicate strong evidence of a correlation between these factors and volume shrinkage. The estimated effects for intracellular and extracellular water were small and highly uncertain (change_intra: −0.21, 95% CI: −1.99 to 1.65; change_extra: 0.32, 95%

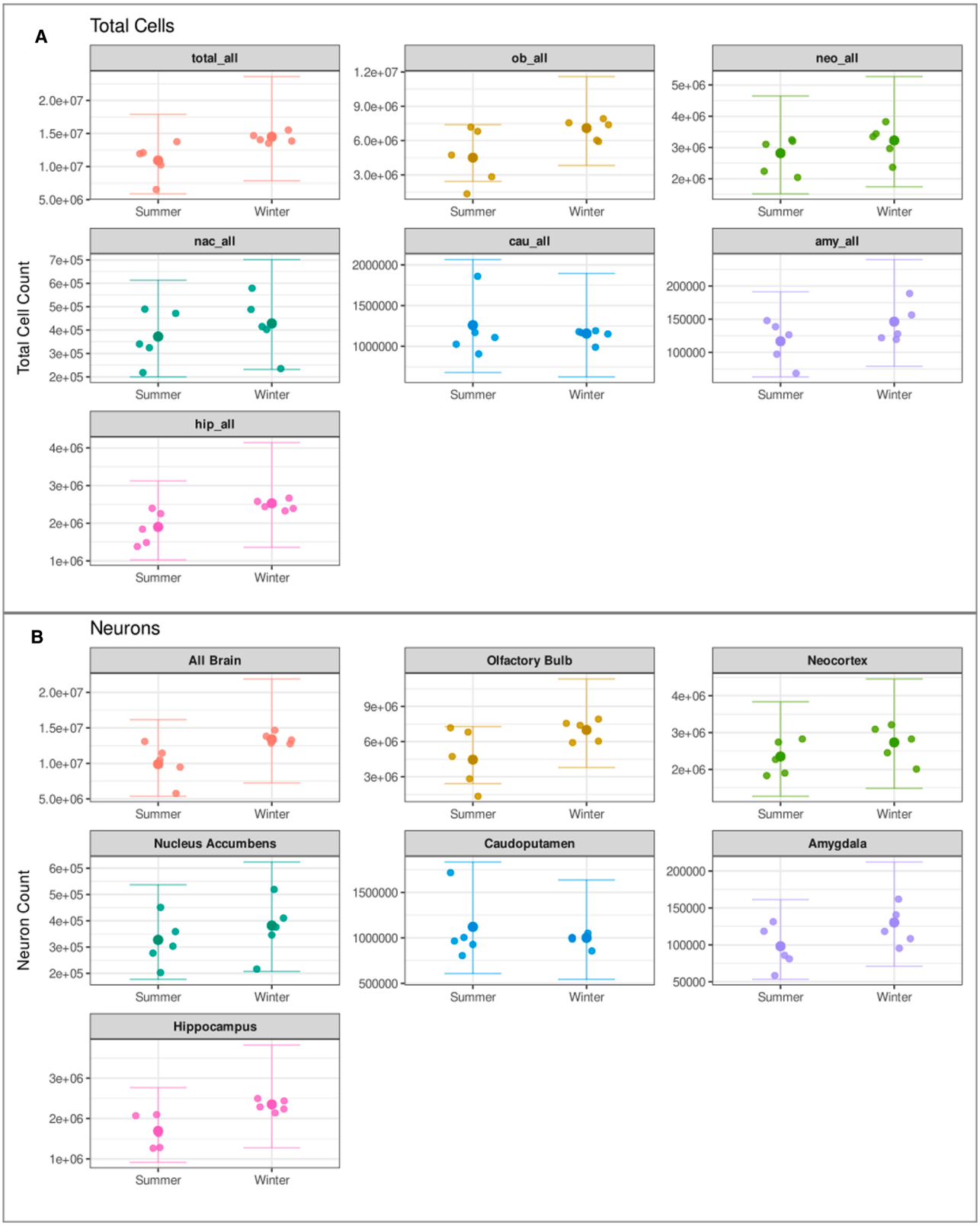

(legend on next page)

CI: −1.24 to 1.85). CSF volume showed no meaningful association with volume change (change_csf: 0.01, 95% CI: −1.87 to 1.93). Results are summarized in the supplemental information (Table S4).

Cell population

We observed a general trend of increased cell population (neurons and glia) from summer to winter across most brain regions. Only the caudoputamen showed a non-significant decrease in cell population from summer to winter. There was a significant increase in cell counts in the olfactory bulb, with winter showing higher counts compared with summer. Although changes in the other regions, including the hippocampus, did not reach statistical significance, the consistent direction of change and visible patterns suggest a potential biological effect. These trends may not have reached significance due to limited statistical power. Counts of neurons, which made up the majority of cells, were estimated with relatively low variance and provide reliable regional comparisons. Glial cells constituted a smaller proportion (~7%) and showed higher variability across samples. Glial counts were not modeled due to greater variability and lower representation. Total cell counts are shown alongside neurons to illustrate general trends while minimizing overinterpretation of glia-specific patterns. All cell count data, including glial estimates by region and season, are freely available in the open repository. Full cell population estimates by region and season are provided in Figure 2.

DISCUSSION

Our study revealed significant seasonal changes in water diffusion properties and brain size in the common shrew. From summer to winter, we observed a 1.08-fold reduction in intracellular water volume fraction across most brain regions, reflecting a broader seasonal adaptation strategy and suggesting that brain shrinkage is driven by cell size reduction rather than cell death.

The observed seasonal changes in diffusion metrics additionally showed shifts in water movement and structure. We observed an increase in MD and rD, indicating that water movement in the extracellular space became less restricted. At the same time, decreases in FA suggested a reduction in the directional movement of water, likely due to structural reorganization within the brain tissue. These changes in water diffusion and structure were accompanied by region-specific alterations in CSF volume, particularly in the cerebellum and hippocampus. Together, these findings point to significant microstructural reconfigurations. This preservation of network integrity allows the shrew brain to maintain function despite volume reduction. As cells lose water, they shrink, increasing extracellular space—a change partially offset by an increase in extracellular water volume. This extracellular expansion helps maintain structural integrity despite volume reduction.

Despite substantial changes in diffusion metrics, changes in neuronal and glial populations remained stable, confirming that brain shrinkage is driven by cell size reduction rather than cell loss. Although the differences between summer and winter were not statistically significant for most regions or for the total brain, we observed a general trend toward increased cell counts in winter. This included a significant increase in the olfactory bulb and non-significant increases in several other regions, such as the cortex, where adult neurogenesis has not been previously documented. The discrepancy from earlier findings[35] may reflect the timing of cell proliferation, which could occur during the shrinkage phase and be completed once minimum brain size is reached.

Despite significant seasonal changes in individual metrics, the proportional relationships between key microstructural components—intracellular, extracellular, and CSF fractions—remained remarkably stable. Similarly, the relationships between FA, aD, and rD exhibited consistent relationships across seasons. This stability was observed in both relative metrics (e.g., proportions of these components within brain regions) and absolute metrics (e.g., volumes calculated by combining these proportions with brain region sizes). These consistent contributions suggest a robust underlying organization that persists across seasons, allowing the brain to maintain functional integrity despite shrinking.[41]

When we compared these metric changes with the observed volume shrinkage, we found no significant correlations. Specifically, variations in intracellular, extracellular, and CSF volumes did not significantly account for the overall reduction in brain volume. This suggests that additional underlying mechanisms may drive the seasonal brain volume changes observed in shrews. The stability of these relationships amid significant changes underscores the brain's structural resilience.[42] Metabolic adjustments may contribute to these stable relationships, such as those involving AQP4, which optimize water management and energy utilization without compromising structural integrity. In addition to AQP4-mediated water redistribution, gene expression data from a previous study[43] indicate that apoptosis-related pathways are downregulated before the onset of winter brain shrinkage. This suggests that programmed cell death is actively suppressed, ensuring that neurons and glia remain viable despite drastic reductions in brain volume. By downregulating apoptosis, shrews preserve their neural networks while allowing for cell shrinkage as an alternative mechanism of metabolic conservation. This further supports the idea that Dehnel's phenomenon is not a degenerative process but a controlled and adaptive strategy for energy efficiency.

Alongside apoptosis downregulation, a seasonal reduction in AQP4 expression has been suggested in the cortex and hippocampus, based on qualitative observations (see supplemental information for details; Figure S3). This reduction could limit water movement from the extracellular to the intracellular space,

Figure 2. Regional differences in brain cell numbers across seasons

Seasonal variation in brain cell numbers across regions.

(A) Total number of cells (neurons + glia) per brain region.

(B) Number of neurons per region. Each point represents one individual. Squares show raw stereologically derived counts, circle and error bars represent posterior means and 95% credible intervals from Bayesian models. Glial cells were counted but not separately modeled due to higher variability and low abundance (~7% of total counts).

contributing to osmotic regulation. Although not quantified here, such a mechanism would be consistent with the observed increase in extracellular water volume fraction and cell shrinkage, supporting the hypothesis that brain volume reductions are driven by water redistribution rather than cell loss. In winter, a possible reduction in AQP4 expression may reflect a reversible and beneficial adaptation. This could help minimize water influx, lower the energy required for ion regulation, and maintain solute balance in the extracellular space. These adaptations enable shrews to maintain brain functionality and survive the harsh food landscape of winter.[44] Dysregulated AQP4 expression in human neurodegenerative conditions, such as Alzheimer's disease, disrupts water and solute balance, leading to β-amyloid deposition and cognitive impairment.[45] Although both shrews and neurodegenerative patients exhibit cortical atrophy and cognitive decline, these changes are adaptive and reversible in shrews. Seasonal dendritic retraction in the hippocampus during winter reduces metabolic demands, while regrowth in spring restores connectivity and cognitive function.[34] This contrasts sharply with the irreversible damage and structural degeneration seen in neurodegenerative diseases, highlighting the adaptive plasticity and resilience of the shrew brain.

One notable aspect of our findings is the variability in response across different brain regions. Our volumetric analysis confirms that seasonal brain shrinkage is not limited to total brain volume but also affects specific regions to varying degrees. This pattern supports the idea that brain plasticity during Dehnel's phenomenon is both systemic and targeted. Although intracellular and extracellular water volume fractions changed in almost all regions, with the direction consistent with overall brain shrinkage, the neocortex and cerebellum exhibited opposite trends. Although AQP4 expression in the neocortex follows the same seasonal reduction observed in other regions, diffusion metrics reveal a more stable microstructural environment. This suggests that maintaining connectivity for sensory integration and higher cognitive function takes precedence over purely metabolic reductions in this region.[46,47] Similarly, the cerebellum, essential for motor coordination and balance, might prioritize structural integrity to ensure efficient motor performance, even after seasonal shrinkage.[48] These findings underscore the importance of regional specialization in optimizing brain adaptation strategies, where different areas balance energy demands and functional priorities to enhance survival under changing environmental conditions.

Exploring the variability in brain region responses to seasonal changes offers valuable insights into the brain's adaptive mechanisms. A regional differential response underscores the importance of considering regional differences in brain structure and function studies. Our findings indicate that adaptation to seasonal demands is not uniformly distributed across the brain. Instead, it involves a complex balance between maintaining structural integrity, meeting functional demands, and managing metabolic needs. Such regional specificity suggests that certain brain areas may have evolved distinct strategies to optimize survival during environmental changes.

Overall, our findings reveal the complexity of seasonal brain plasticity in the common shrew, involving molecular, cellular, structural, and metabolic mechanisms, enabling functional preservation despite significant volume reduction. However, it is crucial to recognize the limitations inherent in the diffusion MRI techniques we employed. For example, factors such as FA can be affected by changes in cellular organization and water content and by variations in brain temperature. Temperature fluctuations can alter the physical properties of cellular membranes and the viscosity of the intracellular environment, which, in turn, affects the diffusion behavior of water molecules measured by FA.[49,50] Such temperature-induced changes could potentially bias the results, leading to misinterpretations of the underlying microstructural integrity. To overcome these limitations and build a more comprehensive model of brain structural adaptations, future research should integrate additional imaging modalities, such as fMRI, and physiological measurements that can capture a broader spectrum of changes.

Although our study focused on the shrinkage phase, previous work suggests that the spring regrowth may reverse these microstructural and molecular changes. This seasonal reversal could serve as a valuable model for studying regenerative processes in the adult brain, offering new perspectives on how structural plasticity might be harnessed to promote recovery or resilience in neurodegenerative conditions.

To our knowledge, no other mammalian brain adaptation has been shown to combine seasonal cell shrinkage, ongoing cell generation, downregulated apoptosis, and possible seasonal changes in AQP4 expression. This exceptional strategy challenges conventional views on brain plasticity and provides a rare example of a controlled, reversible shift in neural architecture.

RESOURCE AVAILABILITY

Lead contact

Further information and requests should be directed to the lead contact, Cecilia Baldoni (cbaldoni@ab.mpg.de).

Materials availability

This study did not generate new unique materials.

Data and code availability

- CSV files including all data have been deposited at Edmond (https://doi.org/10.17617/3.J8V4QU) and are publicly available as of the date of publication.
- All original code has been deposited at Edmond and is publicly available at https://doi.org/10.17617/3.J8V4QU as of the date of publication.
- Any additional information required to interpret the data is available at the Edmond repository: https://doi.org/10.17617/3.J8V4QU.

ACKNOWLEDGMENTS

We would like to thank PD Dr. Irmgard Amrein and her team from the University of Zurich for the use of their stereology equipment and their vast knowledge of cell counting, Marion Muturi and Ivan Lenzi for their help during fieldwork and lab work, the animal caretakers of the Max Plank Institute of Animal Behavior, and Drs. Daniel Zuniga and Inge Müller, who provided incredible help with shrew care. Furthermore, the authors wish to thank the core facility AMIR CF (DFG-RIsources no. RI_00052) for MRI support.

This work was funded by the Human Frontiers Research Grant RGP0013/2019 to D.K.N.D., L.M.D., and J.N. W.R.T. was supported in part by a Stony Brook University Presidential Innovation and Excellence Award to L.M.D.

AUTHOR CONTRIBUTIONS

C.B., D.v.E., and D.K.N.D. conceived the study. B.S., J.L., and M.H. collected histological data (cell counts). D.K.N.D., L.M.D., and J.N. acquired funding.

Y.Z. collected and prepared figures on AQP4. C.B. and M.R. collected and analyzed MRI data. C.B. prepared statistical figures. D.v.E. and M.R. prepared MRI example figures. C.B., M.R., Y.Z., D.v.E., and D.K.N.D. wrote the first draft of the manuscript. All authors contributed to the final manuscript.

DECLARATION OF INTERESTS

The authors declare no competing interests.

STAR★METHODS

Detailed methods are provided in the online version of this paper and include the following:

- KEY RESOURCES TABLE
- EXPERIMENTAL MODEL AND STUDY PARTICIPANT DETAIL
- METHOD DETAILS
  - MRI data acquisition and post-processing
  - Seasonal changes in brain and regional volumes
  - Cell count and tissue histology
  - Tissue processing for AQP4 staining
  - Immunofluorescence staining
  - Correlation between AQP4 expression and seasonal changes
- QUANTIFICATION AND STATISTICAL ANALYSES

SUPPLEMENTAL INFORMATION

Supplemental information can be found online at https://doi.org/10.1016/j.cub.2025.08.015.

Received: March 3, 2025
Revised: June 18, 2025
Accepted: August 11, 2025
Published: September 1, 2025

REFERENCES

1. Kempermann, G. (2012). New neurons for "survival of the fittest". Nat. Rev. Neurosci. *13*, 727–736. https://doi.org/10.1038/nrn3319.
2. Rymer, T., Pillay, N., and Schradin, C. (2013). Extinction or survival? Behavioral flexibility in response to environmental change in the African striped mouse rhabdomys. Sustainability *5*, 163–186. https://doi.org/10.3390/su5010163.
3. Lambert, K., Eisch, A.J., Galea, L.A.M., Kempermann, G., and Merzenich, M. (2019). Optimizing brain performance: identifying mechanisms of adaptive neurobiological plasticity. Neurosci. Biobehav. Rev. *105*, 60–71. https://doi.org/10.1016/j.neubiorev.2019.06.033.
4. Kolb, B., and Gibb, R. (2014). Searching for the principles of brain plasticity and behavior. Cortex *58*, 251–260. https://doi.org/10.1016/j.cortex.2013.11.012.
5. Mateos-Aparicio, P., and Rodríguez-Moreno, A. (2019). The impact of studying brain plasticity. Front. Cell. Neurosci. *13*, 66. https://doi.org/10.3389/fncel.2019.00066.
6. Dehnel, A. (1949). Studies on the genus sorex L. Ann. Univ. M. Curie-Sklod. *4*, 18–102.
7. Bielak, T., and Pucek, Z. (1960). Seasonal changes in the brain weight of the common shrew (Sorex araneus araneus Linnaeus, 1758). Acta Theriol. (Warsz) *3*, 297–300.
8. Lázaro, J., and Dechmann, D.K.N. (2021). Dehnel's phenomenon. Curr. Biol. *31*, R463–R465. https://doi.org/10.1016/j.cub.2021.04.006.
9. Churchfield, S. (1982). Food availability and the diet of the common shrew, Sorex araneus, in Britain. J. Anim. Ecol. *51*, 15–28. https://doi.org/10.2307/4307.
10. Schaeffer, P.J., O'Mara, M.T., Breiholz, J., Keicher, L., Lázaro, J., Muturi, M., and Dechmann, D.K.N. (2020). Metabolic rate in common shrews is unaffected by temperature, leading to lower energetic costs through seasonal size reduction. R. Soc. Open Sci. *7*, 191989. https://doi.org/10.1098/rsos.191989.
11. Keicher, L., O'Mara, M.T., Voigt, C.C., and Dechmann, D.K.N. (2017). Stable carbon isotopes in breath reveal fast incorporation rates and seasonally variable but rapid fat turnover in the common shrew (Sorex araneus). J. Exp. Biol. *220*, 2834–2841.
12. Nováková, L., Lázaro, J., Muturi, M., Dullin, C., and Dechmann, D.K.N. (2022). Winter conditions, not resource availability alone, may drive reversible seasonal skull size changes in moles. R. Soc. Open Sci. *9*, 220652. https://doi.org/10.1098/rsos.220652.
13. LaPoint, S., Keicher, L., Wikelski, M., Zub, K., and Dechmann, D.K.N. (2017). Growth overshoot and seasonal size changes in the skulls of two weasel species. R. Soc. Open Sci. *4*, 160947. https://doi.org/10.1098/rsos.160947.
14. Churchfield, S. (1990). The Natural History of Shrews (Cornell University Press).
15. Mulvey, J., Pillay, N., Makuya, L., Rödel, H.G., and Schradin, C. (2024). African striped mice have relatively smaller brains in the food deprived dry season than in the wet season. Mamm. Biol. *104*, 15–24. https://doi.org/10.1007/s42991-023-00383-2.
16. Zuercher, G.L., Roby, D.D., and Rexstad, E.A. (1999). Seasonal changes in body mass, composition, and organs of northern red-backed voles in interior Alaska. J. Mammal. *80*, 443–459. https://doi.org/10.2307/1383292.
17. Lázaro, J., Dechmann, D.K.N., LaPoint, S., Wikelski, M., and Hertel, M. (2017). Profound reversible seasonal changes of individual skull size in a mammal. Curr. Biol. *27*, R1106–R1107. https://doi.org/10.1016/j.cub.2017.08.055.
18. Pucek, M. (1965). Water contents and seasonal changes of the brain-weight in shrews. Acta Theriol. (Warsz) *10*, 353–367. https://doi.org/10.4098/AT.arch.65-30.
19. Lázaro, J., Hertel, M., Sherwood, C.C., Muturi, M., and Dechmann, D.K.N. (2018). Profound seasonal changes in brain size and architecture in the common shrew. Brain Struct. Funct. *223*, 2823–2840. https://doi.org/10.1007/s00429-018-1666-5.
20. Iliff, J.J., Wang, M., Liao, Y., Plogg, B.A., Peng, W., Gundersen, G.A., Benveniste, H., Vates, G.E., Deane, R., Goldman, S.A., et al. (2012). A paravascular pathway facilitates CSF flow through the brain parenchyma and the clearance of interstitial solutes, including amyloid β. Sci. Transl. Med. *4*, 147ra111. https://doi.org/10.1126/scitranslmed.3003748.
21. Jessen, N.A., Munk, A.S.F., Lundgaard, I., and Nedergaard, M. (2015). The glymphatic system: a beginner's guide. Neurochem. Res. *40*, 2583–2599. https://doi.org/10.1007/s11064-015-1581-6.
22. Rasmussen, M.K., Mestre, H., and Nedergaard, M. (2018). The glymphatic pathway in neurological disorders. Lancet Neurol. *17*, 1016–1024. https://doi.org/10.1016/S1474-4422(18)30318-1.
23. Reeves, B.C., Karimy, J.K., Kundishora, A.J., Mestre, H., Cerci, H.M., Matouk, C., Alper, S.L., Lundgaard, I., Nedergaard, M., and Kahle, K.T. (2020). Glymphatic system impairment in Alzheimer's disease and idiopathic normal pressure hydrocephalus. Trends Mol. Med. *26*, 285–295. https://doi.org/10.1016/j.molmed.2019.11.008.
24. Huber, V.J., Igarashi, H., Ueki, S., Kwee, I.L., and Nakada, T. (2018). Aquaporin-4 facilitator TGN-073 promotes interstitial fluid circulation within the blood–brain barrier : [17O]H2O JJVCPE MRI study. NeuroReport *29*, 697–703. https://doi.org/10.1097/WNR.0000000000000990.
25. Lewis, S., Dyvorne, H., Cui, Y., and Taouli, B. (2014). Diffusion-weighted imaging of the liver: techniques and applications. Magn. Reson. Imaging Clin. N. Am. *22*, 373–395. https://doi.org/10.1016/j.mric.2014.04.009.
26. Trouard, T.P., Harkins, K.D., Divijak, J.L., Gillies, R.J., and Galons, J.P. (2008). Ischemia-induced changes of intracellular water diffusion in rat glioma cell cultures. Magn. Reson. Med. *60*, 258–264. https://doi.org/10.1002/mrm.21616.
27. Reveley, C., Ye, F.Q., Mars, R.B., Matrov, D., Chudasama, Y., and Leopold, D.A. (2022). Diffusion MRI anisotropy in the cerebral cortex is

determined by unmyelinated tissue features. Nat. Commun. *13*, 6702. https://doi.org/10.1038/s41467-022-34328-z.

28. Cercignani, M., Inglese, M., Pagani, E., Comi, G., and Filippi, M. (2001). Mean diffusivity and fractional anisotropy histograms of patients with multiple sclerosis. AJNR Am. J. Neuroradiol. *22*, 952–958.
29. Zhang, Y., and Burock, M.A. (2020). Diffusion tensor imaging in Parkinson's disease and Parkinsonian syndrome: a systematic review. Front. Neurol. *11*, 531993. https://doi.org/10.3389/fneur.2020.531993.
30. Neukomm, L.J., and Freeman, M.R. (2014). Diverse cellular and molecular modes of axon degeneration. Trends Cell Biol. *24*, 515–523. https://doi.org/10.1016/j.tcb.2014.04.003.
31. Wang, J.T., Medress, Z.A., and Barres, B.A. (2012). Axon degeneration: molecular mechanisms of a self-destruction pathway. J. Cell Biol. *196*, 7–18. https://doi.org/10.1083/jcb.201108111.
32. Gomolka, R.S., Hablitz, L.M., Mestre, H., Giannetto, M., Du, T., Hauglund, N. L., Xie, L., Peng, W., Martinez, P.M., Nedergaard, M., et al. (2023). Loss of aquaporin-4 results in glymphatic system dysfunction via brain-wide interstitial fluid stagnation. eLife *12*, e82232. https://doi.org/10.7554/eLife.82232.
33. Baldoni, C., Raptis, K., Farantouri, M., Lenzi, I., Lim, K.S., Menz, M.H.M., Muturi, M., Reisert, M., Bedoya Duque, M.A., Thomas, W.R., et al. (2025). Captivity alters behaviour but not seasonal brain size change in semi-naturally housed shrews. R. Soc. Open Sci. *12*, 242138. https://doi.org/10.1098/rsos.242138.
34. Lázaro, J., Hertel, M., LaPoint, S., Wikelski, M., Stiehler, M., and Dechmann, D.K.N. (2018). Cognitive skills of common shrews (Sorex araneus) vary with seasonal changes in skull size and brain mass. J. Exp. Biol. *221*, jeb166595.
35. Bartkowska, K., Djavadian, R.L., Taylor, J.R.E., and Turlejski, K. (2008). Generation recruitment and death of brain cells throughout the life cycle of Sorex shrews (Lipotyphla). Eur. J. Neurosci. *27*, 1710–1721. https://doi.org/10.1111/j.1460-9568.2008.06133.x.
36. Lázaro, J., Hertel, M., Muturi, M., and Dechmann, D.K.N. (2019). Seasonal reversible size changes in the braincase and mass of common shrews are flexibly modified by environmental conditions. Sci. Rep. *9*, 2489. https://doi.org/10.1038/s41598-019-38884-1.
37. Pucek, Z., and Pucek, Z. (1963). Seasonal changes in the braincase of some representatives of the genus Sorex from the Palearctic. J. Mammal. *44*, 523–536. https://doi.org/10.2307/1377135.
38. Kellner, E., Reisert, M., Rau, A., Hosp, J., Demerath, T., Weiller, C., and Urbach, H. (2022). Clinical feasibility of diffusion microstructure imaging (DMI) in acute ischemic stroke. NeuroImage Clin. *36*, 103189. https://doi.org/10.1016/j.nicl.2022.103189.
39. Ganepola, T., Nagy, Z., Ghosh, A., Papadopoulo, T., Alexander, D.C., and Sereno, M.I. (2018). Using diffusion MRI to discriminate areas of cortical grey matter. NeuroImage *182*, 456–468. https://doi.org/10.1016/j.neuroimage.2017.12.046.
40. Ganepola, T., Lee, Y., Alexander, D.C., Sereno, M.I., and Nagy, Z. (2021). Multiple b-values improve discrimination of cortical gray matter regions using diffusion MRI: an experimental validation with a data-driven approach. MAGMA *34*, 677–687. https://doi.org/10.1007/s10334-021-00914-3.
41. Assaf, Y., and Pasternak, O. (2008). Diffusion tensor imaging (DTI)-based white matter mapping in brain research: a review. J. Mol. Neurosci. *34*, 51–61. https://doi.org/10.1007/s12031-007-0029-0.
42. Budde, M.D., Kim, J.H., Liang, H.F., Schmidt, R.E., Russell, J.H., Cross, A. H., and Song, S.K. (2007). Toward accurate diagnosis of white matter pathology using diffusion tensor imaging. Magn. Reson. Med. *57*, 688–695. https://doi.org/10.1002/mrm.21200.
43. Thomas, W.R., Richter, T., O'Neil, E.T., Baldoni, C., Corthals, A.P., von Elverfeldt, D., Nieland, J.D., Dechmann, D., Hunter, R., and Davalos, L. M. (2025). Seasonal and comparative evidence of adaptive gene expression in mammalian brain size plasticity. eLife *13*, RP100788.
44. Churchfield, S., Rychlik, L., and Taylor, J.R.E. (2012). Food resources and foraging habits of the common shrew, Sorex araneus: does winter food shortage explain Dehnel's phenomenon? Oikos *121*, 1593–1602. https://doi.org/10.1111/j.1600-0706.2011.20462.x.
45. Simon, M., Wang, M.X., Ismail, O., Braun, M., Schindler, A.G., Reemmer, J., Wang, Z., Haveliwala, M.A., O'Boyle, R.P., Han, W.Y., et al. (2022). Loss of perivascular aquaporin-4 localization impairs glymphatic exchange and promotes amyloid β plaque formation in mice. Alzheimers Res. Ther. *14*, 59. https://doi.org/10.1186/s13195-022-00999-5.
46. Caroni, P., Donato, F., and Muller, D. (2012). Structural plasticity upon learning: regulation and functions. Nat. Rev. Neurosci. *13*, 478–490. https://doi.org/10.1038/nrn3258.
47. Holtmaat, A., and Svoboda, K. (2009). Experience-dependent structural synaptic plasticity in the mammalian brain. Nat. Rev. Neurosci. *10*, 647–658. https://doi.org/10.1038/nrn2699.
48. D'Angelo, E., and Casali, S. (2012). Seeking a unified framework for cerebellar function and dysfunction: from circuit operations to cognition. Front. Neural Circuits *6*, 116. https://doi.org/10.3389/fncir.2012.00116.
49. Berger, C., Bauer, M., Wittig, H., Scheurer, E., and Lenz, C. (2022). Post mortem brain temperature and its influence on quantitative MRI of the brain. MAGMA *35*, 375–387. https://doi.org/10.1007/s10334-021-00971-8.
50. Bertalan, G., Boehm-Sturm, P., Schreyer, S., Morr, A.S., Steiner, B., Tzschätzsch, H., Braun, J., Guo, J., and Sack, I. (2019). The influence of body temperature on tissue stiffness, blood perfusion, and water diffusion in the mouse brain. Acta Biomater. *96*, 412–420. https://doi.org/10.1016/j.actbio.2019.06.034.
51. Veraart, J., Novikov, D.S., Christiaens, D., Ades-Aron, B., Sijbers, J., and Fieremans, E. (2016). Denoising of diffusion MRI using random matrix theory. Neuroimage *142*, 394–406.
52. Kellner, E., Dhital, B., Kiselev, V.G., and Reisert, M. (2016). Gibbs-ringing artifact removal based on local subvoxel-shifts. Magnetic resonance in medicine *76*, 1574–1581.
53. Zhang, H., Schneider, T., Wheeler-Kingshott, C.A., and Alexander, D.C. (2012). NODDI: practical in vivo neurite orientation dispersion and density imaging of the human brain. Neuroimage *61*, 1000–1016.
54. Reisert, M., Kellner, E., Dhital, B., Hennig, J., and Kiselev, V.G. (2017). Disentangling micro from mesostructure by diffusion MRI: a Bayesian approach. NeuroImage *147*, 964–975.
55. Novikov, D.S., Fieremans, E., Jespersen, S.N., and Kiselev, V.G. (2019). Quantifying brain microstructure with diffusion MRI: Theory and parameter estimation. NMR in Biomedicine *32*, e3998.
56. Baldoni, C., Thomas, W.R., von Elverfeldt, D., Reisert, M., Làzaro, J., Muturi, M., Dávalos, L.M., Nieland, J.D., and Dechmann, D.K. (2023). Histological and MRI brain atlas of the common shrew, Sorex araneus, with brain region-specific gene expression profiles. Frontiers in Neuroanatomy *17*, 1168523.
57. Burke, M.W., Ptito, M., Ervin, F.R., and Palmour, R.M. (2015). Hippocampal neuron populations are reduced in vervet monkeys with fetal alcohol exposure. Dev. Psychobiol. *57*, 470–485.
58. West, M.J., Slomianka, L., and Gundersen, H.J.G. (1991). Unbiased Stereological Estimation of the Total Number of Neurons in the Subdivisions of the Rat Hippocampus Using the Optical Fractionator. Anat. Rec. *231*, 482–497.
59. West, M.J. (2001). Design based stereological methods for estimating the total number of objects in histological material. Folia Morphol. (Warsz). *60*, 11–19.
60. Cotter, D., Mackay, D., Landau, S., Kerwin, R., and Everall, I. (2001). Reduced Glial Cell Density and Neuronal Size in the Anterior Cingulate Cortex in Major Depressive Disorder. Arch. Gen. Psychiatry *58*, 545–553.
61. Coppola, G., Di Renzo, A., Tinelli, E., Petolicchio, B., Di Lorenzo, C., Parisi, V., Serrao, M., Calistri, V., Tardioli, S., Cartocci, G., Caramia, F., Di Piero, V., and Pierelli, F. (2020). Patients with chronic migraine without history of medication overuse are characterized by a peculiar white matter fiber bundle profile. The Journal of Headache and Pain *21*, 92. https://doi.org/10.1186/s10194-020-01159-6.

CellPress
OPEN ACCESS

STAR★METHODS

KEY RESOURCES TABLE

REAGENT or RESOURCE	SOURCE	IDENTIFIER
Biological sample		
Common shrew (*Sorex araneus*)	Wild caught, Möggingen, Germany	N/A
Chemicals, peptides, and recombinand proteins		
Cresyl Violet	Sigma-Aldrich	C5042
Sevoflurane	Baxter	N/A
Roti-Histofix	Carl Roth	HP687.1
Softwares and algorithms		
R	CRAN	v4.2.1
Stereo Investigator software	MBF Bioscience	v11.03
NORA imaging platform	nora-imaging.org	nora-imaging.org
Bruker BioSpec 70/20 MRI system	Bruker	N/A
Deposited data		
Raw data and code	Edmond Repository	https://doi.org/10.17617/3.J8V4QU

EXPERIMENTAL MODEL AND STUDY PARTICIPANT DETAIL

All handling and sampling methods were approved by the Regierungspräsidium Freiburg, Baden-Württemberg, Germany (35-9185.81/G-11/21, 35-9185.81/G-19/80 and 35-9185.81/G-22/082).

We caught common shrews (*Sorex araneus*) in wet meadows and wet forest-edge areas in Möggingen, Germany (47°46′04.70″N, 8°59′47.11″E), near the Max Planck Institute of Animal Behavior. We caught shrews using live wooden traps (PPUH A. Marcinkiewicz, Rajgród, Poland)(described in Lázaro et al.[36]). For the cell count, we captured five summer juveniles (males) when their brains were at maximum size, between June and September 2014, and five winter subadults (four males, one female), when the brains were at minimum size, between December 2013 and February 2014. The shrews were sacrificed on the day of capture by perfusion through the heart under deep anesthesia, to remove blood from the brain and other organs. Sex was determined during dissections by the presence of testes or ovaries. The extracted brains were weighed and placed into 4% formaldehyde for storage.

For the DMI study, we caught 19 summer juveniles in August 2021 and kept them in captivity for six months until February 2022. As is typical for this species, mortality occurred in autumn,[14] and by February 2022, our captive group had been reduced to seven individuals. All shrews were housed individually in a double-cage system (see Baldoni et al.[33] for details), in an outdoor aviary with natural light, temperature, and humidity.

METHOD DETAILS

MRI data acquisition and post-processing

All MR imaging was performed at the Universitätsklinikum Freiburg, Germany using a dedicated small animal MRI system (BioSpec 70/20 | Bruker, Germany) using a cryogenically cooled, two-element transmit/receive surface mouse head coil. Animals were anaesthetized in a knockdown box heated by a warming mat under the thorax to maintain body temperature. They were given 4.5 Vol% Sevoflurane in 1l/min O_2 gas. We then placed the animals into the animal bed, fixated them with sticky tape, applied ointment (Bepanthen®) to the eyes to prevent drying, and transferred them into the MRI scanner. During pilot-, morphology- and diffusion weighted-scanning anaesthesia was upheld with 2.5 Vol% Sevoflurane in a mixture of 0.8 l/min air and 0.4 l/min O_2.

Morphology was depicted using a T2-weighted 2D TurboRARE pulse sequence covering the complete brain. The sequence consisted of 40 slices 300 μm thick, with a field of view of 16x12 mm, a matrix size of 200x160, and an in-plane resolution of 80x80 μm. Acquisition parameters were TE/TR 40ms/5075ms, a RARE-factor of eight, two averages, and a bandwidth of 35 kHz, leading to an acquisition time of approximately three minutes.

Diffusion-weighted imaging was performed as 'high angular resolution diffusion imaging' (HARDI) with two different diffusion weighting values b_1= 1000 s/mm^2 and b_2=1600 s/mm^2, 30 diffusion encoding directions, and four A_0 images. For both scans a four segments, spin echo EPI pulse sequence covering the complete brain with 40 slices, 300 μm thick, a field of view of 15x8 mm, and a matrix size of 100x53 leading to an in-plane resolution of 150x151 μm was employed. A saturation slab ventral of the brain allowed for a smaller FOV in the sagittal direction. A TE/TR of 24ms/2200ms led to a total acquisition time of five minutes for each b-value. We performed all data post-processing on the post-processing platform NORA (www.nora-imaging.org).

Diffusion-weighted images were first denoised,[51] had Gibbs-ringing artifacts corrected.[52] Microstructural diffusion metrics, based on a three-compartment standard white-matter model,[53–55] were estimated via a Bayesian framework.[54] We also computed conventional DTI diffusivity parameters using standard log-linear regression. All dMRI volumes were coregistered to the anatomical TurboRARE images. and the accuracy of these registrations (including alignment with binary masks) was confirmed through visual inspection. For regional segmentation, we used a previously developed brain atlas of the common shrew, generated from high-resolution MRI scans.[56] This atlas allowed consistent delineation of anatomical regions across all subjects and was used for regional analysis and visual overlays on the diffusion maps.

Seasonal changes in brain and regional volumes

To quantify the seasonal shrinkage of total brain volume and regional volumes, we fitted Bayesian Gaussian models using total brain volume as a response variable and season as a predictor, including random intercepts for individual ID. We also fitted separate models for each of the 13 brain regions using the same structure. All models were implemented in brms using weakly informative priors. Model convergence was assessed using standard diagnostics.

Cell count and tissue histology

After extracting the whole brain from the braincase, we weighed it. We then cut and weighed the right hemisphere separately. Next, we placed the right hemisphere into progressively increasing sucrose solutions (10%, 20%, and 30%) until it sank, which prevented damage during freezing. We oriented the hemisphere with the olfactory bulb facing upward, froze it in a small water block, and sectioned it into 30μm slices using a sliding microtome. We stored the sections in a freezing solution (3 parts ddH2O, 3 parts glycerol, 3 parts ethylene glycol, and 1 part phosphate buffer) or a PB (phosphate-buffered saline) solution containing 10% sodium azide.

We performed Nissl staining on every 5th section as follows: we soaked the sections in ddH2O for one minute, then immersed them sequentially in ethanol solutions of increasing concentration (30%, 50%, 70%, 95%, and 100%), spending one minute in each solution. We then transferred the sections to a 50% chloroform/50% ethanol solution for ten minutes, refreshing the solution halfway through. Afterwards, we rehydrated the sections in ethanol solutions of decreasing concentration in reverse order, followed by soaking them in ddH2O for one minute. We stained the sections in Cresyl Violet solution for eight minutes and rinsed them twice in ddH2O for one minute each time. We ascended through ethanol concentrations again, replacing the 95% ethanol step with 95% ethanol containing a small amount of acetic acid. Finally, we treated the sections with Roti histology-clearing agent for five minutes and mounted them using DPX mountant.

After mounting the sections, we observed that they began to shrink slowly. To counter this, we counted each brain series within a week of mounting. We stained and mounted the brains in randomly assorted groups of two or three. To prevent counting bias, we covered the slide labels and assigned temporary identification letters so the counter was unaware of the brain's age group.

We counted cells in the olfactory bulb, neocortex, nucleus accumbens, caudoputamen, amygdala, and hippocampus. Using 4x magnification, we traced the outlines of each region, and at 64x magnification, we counted the cells. After tracing a region, we used the Stereo Investigator 11.03 program to lay down a grid. We determined the grid's square size (step size) for each region by applying the formula below. We then rounded the suggested step size to a lower, simple number. Through trial runs on a single brain, we adjusted the step size as needed. For instance, although a step size of 600μm was calculated for the hippocampus, we reduced it to 500μm after observing cell density variation in this region. Similarly, we adjusted the frequency of counted sections: for the neocortex, with its relatively homogenous cell distribution, we counted every 10th section, while for the hippocampus, with its less homogenous distribution, we counted every 5th section. In regions where we reduced the section frequency to every 10th section, we compensated by halving the "total area" component of the formula.

We selected the size of the counting frame, a 3D cuboid spanning the section's top and bottom focal layers, to contain an average of 1–2 countable cells.[57,58] Short trial runs for each region helped us determine the appropriate size. Based on the results, we assigned a 15x15μm frame size to the neocortex, caudoputamen, nucleus accumbens, amygdala, and hippocampus. For the olfactory bulb, which had higher cell density, we used a smaller 7x7μm frame. After observing that sections shrank from 30μm to approximately 15μm in thickness during trial staining, we set the guard regions to 2μm and the counting frame height to 10μm.

We programmed the Stereo Investigator software to randomly position the counting frame within each grid square at the start of a count. The frame's position varied between counts but remained constant during a single count.[59] The software, in conjunction with the microscope setup, precisely moved the frame to the next counting area within the same region. We classified and counted cells as either neurons or glia. We identified neurons by their single nucleolus, dendrites,[60] larger size, irregular or triangular cytoplasm, and pale staining. We recognized microglia by their small, dark, comma-shaped appearance. We excluded epithelial cells (dark, no nucleus, curved) from counts. We identified oligodendrocytes by their dark staining and smooth, round appearance.[60] Although astrocytes were rare, we recognized them as large, irregularly shaped cells with pale staining. In the olfactory bulb and certain hippocampal layers, we observed a large number of neurons resembling oligodendrocytes: round and darkly stained. In these areas, we counted all such cells as neurons. Finally, we used the Stereo Investigator program to estimate the total cell number based on the region's volume and the counted cells. We weighted the population estimate by the average section thickness and adjusted it for the missing section fraction.

Tissue processing for AQP4 staining

To identify AQP4 expression, equally grouped shrews were euthanized via vascular perfusion with PAXgene Tissue Fixative. Subsequently, the hemispheres were extracted and incubated in PAXgene Tissue Stabilizer, followed by sequential immersion in 10% and

25% sucrose solutions (for 8 hours and overnight, respectively). The samples were stored in 25% sucrose solution with 0.1% NaN in PBS at 4°C for cryoprotection. Frozen brain sections were cut at a thickness of 40 μm and grouped by season. The sections were stored in an antifreeze solution at -18°C for several years without significant loss of immunoreactivity.

Immunofluorescence staining

All sections were rinsed three times with Potassium Phosphate Buffered Solution, followed by permeabilization and blocking with an Incubation Buffer containing 0.3% Triton X and 3% pig serum for 1 hour. The tissues were then incubated with the primary antibody, rabbit anti-AQP4 (1:10,000, Alomone Labs, 249-323), overnight at 4°C. Primary antibodies were detected with Alexa Fluor 594 goat anti-rabbit antibodies (1:1,000, Thermo, A-11037). Nuclei were stained with 4′,6-diamidino-2-phenylindole (DAPI) (1:500, Sigma, D9542) for 5 minutes. After staining, the tissues were mounted on glass slides with fluorescent mounting medium (DAKO, S3023) and imaged using a Zeiss Axio Observer Z1 microscope equipped with a ×20 objective. To ensure consistency, all samples were stained on the same day. Randomly selected images from each group were analyzed using ImageJ software. To verify fixation and perfusion quality, we performed CPT1 staining and DAPI counterstaining on liver tissue from all individuals. Signal quality and tissue morphology were consistent across seasons, confirming adequate perfusion and fixation.

Correlation between AQP4 expression and seasonal changes

Seasonal variations affected AQP4 expression in the cortex and hippocampus. In the cerebral cortex, AQP4 expression declined from summer to winter (Figures S3A and S3B). Throughout both seasons, AQP4 was primarily localized in the cerebral cortex around blood vessels, reflecting its perivascular distribution in the brain (Figure S3A). Nonetheless, in winter, the expression became sparse and scattered. A comparable expression pattern, including sparse winter expression, was observed in the hippocampus (Figure S3B).

QUANTIFICATION AND STATISTICAL ANALYSES

We evaluated the effects of seasonal changes on various brain metrics using a Bayesian hierarchical modelling framework in R (v4.1.2; R Core Team, 2021). Initially, we created models to assess the direct effect of season on various brain metrics and their interactions with each brain region. This allowed us to investigate region-specific seasonal impacts on metrics such as intracellular and extracellular water volume fractions, mean diffusivity (MD), axial diffusivity (aD), radial diffusivity (rD), fractional anisotropy (FA), and cerebrospinal fluid (CSF) volume fraction. We modelled each metric separately to account for their potential different response to seasonal variation. The models were implemented using Stan through the rstan package in R (Stan Development Team, 2024). Visualizations of these distributions and region-specific patterns are provided in Figure S1 (individual distributions) and Figure S2 (region-level model output). Complete model estimates are reported in Table S1.

Next, we extended the analysis to examine how the correlation between metrics of interest varied between seasons. With this analysis we aimed to understand whether the relationship between these metrics differed significantly with seasonal variation, potentially indicating a seasonal modulation of brain physiology. To do this, we implemented a Bayesian hierarchical model to investigate the relationship between CSF, intracellular and extracellular water volume fraction, and the relationship between FA, aD and rD. Changes in FA are closely associated with alterations in aD and rD, indicative of myelin and axonal damage, respectively.[61] Regression model results for these analyses are reported in Tables S2 and S3, respectively.

Additionally, we created a separate model using the absolute values, obtained by multiplying the relative metric proportions by the corresponding brain region volume. These metrics provide a measure of the actual volume occupied by each component within the brain region, offering a more direct quantification of changes in brain tissue. Lastly, we aimed to determine if changes in microstructural metrics (intracellular - extracellular water volume fraction and CSF) correlated with the observed volume shrinkage from summer to winter. The model results for these analyses are included in Table S4.

We conducted a regression analysis to understand if and how the cell population changed across different regions between the summer and winter groups. Hypothesis testing was performed to compare the differences in cell counts for each region by calculating the posterior estimates, standard errors, and credible intervals between the summer and winter groups. For all models, we assessed model stability and convergence with standard diagnostic metrics: effective sample sizes (n_eff), the Gelman-Rubin convergence statistic (Rhat) and Pareto k diagnostics. We used posterior predictive check functions to assess model fit visually.